https://doi.org/10.3311/PPci.24748

Periodica Polytechnica Civil Engineering, 68(3), pp. 987–998, 2024

Formation Mechanism of Rail Corrugation for Modern Tram Lines

Zhiqiang Wang[1*], Zhenyu Lei[1], Jianyue Zhu[1,2]

[1] Institute of Rail Transit, Tongji University, No. 4800 Cao'an Road, Jiading District, 201804 Shanghai, China
[2] State Key Laboratory of Rail Transit Vehicle System, Southwest Jiaotong University, Jiuli Campus, No. 111, North Section 1, Second Ring Road, 610031 Chengdu, China
[*] Corresponding author, e-mail: wangzq@tongji.edu.cn

Received: 28 December 2023, Accepted: 24 March 2024, Published online: 23 May 2024

Abstract

In order to explain the phenomenon of corrugation on measured line sections of the modern tram, a numerical model of modern tram-track coupling has been established by utilizing the multi-body dynamics method, and the formation mechanism of corrugation has been studied from the perspective of wheel-rail contact creep. The results show that the smaller the curve radius is, the greater the probability of corrugation occurs. The corrugation wavelength range is 40 mm~50 mm, the wave depth range is 0.05 mm~0.1 mm, and the wave depth is relatively small compared with the corrugation wave depth of metro lines, which is in line with the characteristics of the light-load operation of the tram. The formation mechanism of corrugation on modern tram sharp curves can be described as wheel-rail contact creep saturation leads to the generation of corrugation, and the source of creep is related to the guiding mechanism of the longitudinally coupled independent wheelset bogie. The formation of corrugation on the straight line of the modern tram is related to the difference in wheel diameters between the front and rear wheelsets on the same side, which can lead to different longitudinal velocities, thus generating longitudinal creep forces and inducing rail corrugation.

Keywords

modern tram, rail corrugation, multi-body dynamics, contact creep, wheel diameter difference

1 Introduction

Rail corrugation is prevalent in the railroad system, mainly manifested as wave-like unevenness along the longitudinal direction of the rail surface. The occurrence of rail corrugation is closely related to the dynamics of vehicle-track system, therefore, for different vehicle operating environments, the occurrence probability and apparent characteristics of rail corrugation are not the same [1]. Rail corrugation is very easy to induce abnormal vibration and high-frequency noise in the wheel-rail system, damaging system components and adversely affecting the stability of vehicle operation [2, 3]. At the present stage, the research on rail corrugation is mainly concentrated in the metro line, which is due to the metro system with many small radius curves, frequent starting and braking, the complexity of track structures and other objective factors [4–6], and the relevant results have certain positive significance for the understanding of the mechanism of metro corrugation and the control of the corrugation evolution [7, 8].

Similar to metro systems, the phenomenon of rail corrugation also occurs in tram lines, but the theoretical analysis of the cause of the latter has been rarely reported. Compared with metro lines, tram lines have specific modes of operation and structural types, which lead to the formation mechanism of rail corrugation on such lines that may be different from the existing rail corrugation theories. Therefore, in order to ensure the normal operation of the tram transportation system, the corrugation cause needs to be analyzed. In the meantime, exploring the effective treatment method of rail corrugation has always been one of the important topics in the railroad industry, and understanding the formation mechanism of rail corrugation is the necessary precondition for realizing the control of corrugation.

Theoretical analysis and experimental measurements are the main methods used in the research of rail corrugation. Based on literature investigation and engineering

Cite this article as: Wang, Z., Lei, Z., Zhu, J. "Formation Mechanism of Rail Corrugation for Modern Tram Lines", Periodica Polytechnica Civil Engineering, 68(3), pp. 987–998, 2024. https://doi.org/10.3311/PPci.24748

experience, Grassie and Kalousek [9] first systematically classified rail corrugation, determined the wavelength-fixing mechanism and damage mechanism of corrugation occurrence, and gave the corresponding control measures. Later, Grassie [10] amended the wavelength-fixing mechanism to the frequency-fixing mechanism and guided the implementation of relevant engineering projects accordingly [11, 12]. Chen et al. [13–15] put forward the viewpoint that friction self-excited vibration triggered rail corrugation, and verified the validity of the above viewpoint in combination with field measurements. The theory of friction self-excited vibration is able to accurately capture the system's destabilization-sensitive frequencies and therefore explains rail corrugation on many lines. Matsumoto et al. [16] interpreted the cause of corrugation on the curve track as the wheel-rail contact stick-slip vibration and analyzed the growth process of corrugation by bench tests, line tests and numerical simulations. Wu [17] analyzed the formation process of rail corrugation utilizing the numerical method, and found that rail corrugation caused by the uneven wear was related to the variation law of wheel-rail interaction resulted from the parameter excitation, and the wheel-rail parameter excitation could directly cause rail corrugation.

For the rail corrugation on the tram line, the existing literatures mainly focus on its measurement methods and the responses of induced vibration and noise. Chiacchiari and Loprencipe [18] discussed the measurement techniques for rail corrugation and proposed an analysis method for the processing of the measured data of rail profiles. Kou et al. [19] used image processing and supervised learning algorithms to assess the damage level of the rail surface and achieved a good prediction for the damage. Herráiz et al. [20] reproduced the vibration behaviors of a real tram track using an analytical model, where the dynamic loads generated by the corrugation were calculated by an auxiliary model and then fed back to the main model to obtain the generated vibrations, which were transferred to the track. Bethel Lulu et al. [21] employed a pseudo-excitation method to study the random vibration characteristics of tram-track interaction on the curve track due to polygonal wheels and track irregularities. The results demonstrated that under the polygonal wheel excitation, wheelset flexibility exacerbated the vibration levels of the track, car body and axlebox, as well as the wheel-rail contact force and creepage. Based on the tram noise calculation model and equivalent noise level measurements, Mandula et al. [22] constructed an improved calculation model for predicting the noise level of the tram. Csortos et al. [23] analyzed the necessary of using rail lubrication on tram tracks and investigated the type and application amounts of lubricants so as to obtain a satisfactory noise reduction. In addition, through indoor and field measurements, Csortos et al. [24] evaluated the effect of rail dampers for vibration and noise reduction, and the results showed that rail web elements could be used for rolling noise reduction and vibration attenuation in most cases. Jóvér and Fischer [25] examined track geometry parameters of the superstructure of the tram Line 1 in Budapest by means of field measurements and numerical calculations for determining the life cycle. Further, Jóvér et al. [26] carried out a detailed comparison of paved tram superstructure systems in terms of track geometry, track gross passing weight and service life of the track section.

As an indispensable part of the modern transportation system, the tram eases the traffic pressure in the city on the one hand and promotes the sustainable development of the city on the other hand. However, the emergence of rail corrugation has brought about a number of adverse effects on the tram system. The existing literatures mainly concentrate on the cause of rail corrugation on metro lines, while less about the cause of rail corrugation on tram lines. With the background of the actual engineering project, this paper investigates the phenomenon of rail corrugation on modern tram lines, with a view to explaining the formation mechanism of rail corrugation on the line. Firstly, the field investigation of rail corrugation is specifically introduced, and the occurrence features of rail corrugation are summarized. Then, with reference to the modern tram line system, a modern tram-track coupling numerical model is established using the multi-body dynamics method. Finally, the formation mechanism of rail corrugation on the modern tram line is analyzed from the perspective of contact creep. This study further complements the theoretical framework of rail corrugation and is useful for understanding and controlling rail corrugation on tram lines.

2 Field investigation of rail corrugation

The investigation line is Huai'an Modern Tram Line No. 1, which was opened in December 2015, with the upstream starting from the Stadium Station and ending at the South Gate Station, and the total length of the main line is 20.07 km (double lines, of which the upstream and downstream lines are 20.07 km each). The Huai'an modern tram is articulated 100% low-floor vehicles, the whole line is the monolithic track slab, and the rails are uniformly made of the high-strength steel with the material of U75V, and

the track stiffness is basically the same. This investigation mainly aims at typicality screening for different curve radius sections, in accordance with the principle of selecting 4 lines for the curve radius below 50 m, 3 lines for the curve radius 51–400 m, and 2 lines for the curve radius above 401 m, and increasing the selection of 2 reverse curves, a total of 11 representative curves are selected for field measurements, and the distribution situation of the lines is as shown in Fig. 1.

As can be seen from Fig. 1, on the 11 lines investigated, a total of 4 lines appear rail corrugation, including 1 reverse curve, 2 lines with the curve radius of less than 50 m and 1 line with the curve radius of 51~400 m. Moreover, when the curve radius is greater than 400 m, rail corrugation rarely occurs on the line. Further, four representative sets of line sections are selected for corrugation measurements and the relevant results are described below:

1. The first set of line section is a circular curve with a curve radius of 30 m. There is corrugation on both the inner and outer rails of the line, with a wavelength of 40 mm and a wave depth of 0.06 mm measured by the Corrugation Analysis Trolley (the validity of this method has been widely verified [27, 28]), and the overall length of corrugation is about 20 m. The field picture of rail corrugation is shown in Fig. 2.
2. The second set of line section is a circular curve with a curve radius of 105 m. There is corrugation on both the inner and outer rails of the line, with a wavelength of 40 mm and a wave depth of 0.05 mm, and the overall length of corrugation is about 35 m. The corresponding field picture of rail corrugation is shown in Fig. 3.

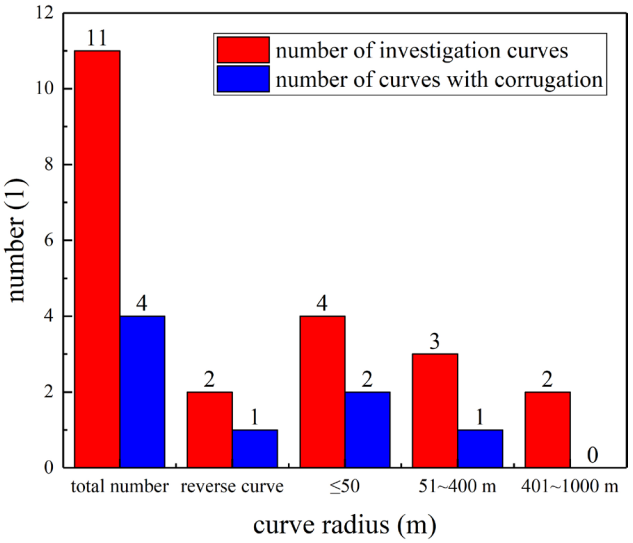

Fig. 1 Distribution situation of investigation lines

Fig. 2 Outer rail corrugation on line section 1

Fig. 3 Inner rail corrugation on line section 2

3. The third set of line section is a straight line. There is corrugation on both the left and right rails, with a wavelength of 50 mm and a wave depth of 0.1 mm, and the overall length of corrugation is about 50 m. The field picture of rail corrugation is shown in Fig. 4.

Fig. 4 Rail corrugation on line section 3

4. The fourth set of line section is a circular curve with a curve radius of 350 m. There is corrugation on the outer rail of the line, with a wavelength of 50 mm and a wave depth of 0.07 mm, and the overall length of corrugation is about 50 m. The corresponding field picture is shown in Fig. 5.

In general, rail corrugation of modern tram lines is mainly concentrated in the small radius curve section with the radius below 400 m. The wavelength range is 40 mm~50 mm, the wave depth range is 0.05 mm~0.1 mm, and the wave depth is relatively small compared with that of metro lines, which is in line with the characteristics of light-load operation of the tram.

Fig. 5 Outer rail corrugation on line section 4

3 Multi-body dynamics numerical model

Based on the actual line situation, this section establishes a vehicle-track coupling numerical model applicable to the modern tram line by using the multi-body dynamics method, which includes a train module, a track module and a wheel-rail contact module. The train module consists of car bodies, bogies and wheelsets, and connects car bodies to bogies and bogies to wheelsets by means of secondary and primary suspensions. The train bogie is the independent wheelset bogie, the configuration form is three motors and one trailer, as shown in Fig. 6 [29], in which the left and right head cars are motors, and the middle two cars are one motor and one trailer. The motor bogie is front and rear coupled (i.e., longitudinally coupled), which is different from the left and right coupling of the traditional bogie wheelset, and there is no coupling device between the left and right wheels, which can be independently rotated through the connection of the axle bridge. The two wheels at the front and rear of the same side of the bogie are longitudinally coupled through the motor, coupling, and output shaft, etc. The bogie motor is controlled in parallel with the rack control, so that the front and rear wheels have the same angular velocity. The four wheels of the trailer bogie are free wheels, uncoupled from each other and able to rotate completely independently. The wheel tread consists of curve segments of R15, R80, R330 and straight line segments of 1:40 and 1:20, in which the rim height is 22 mm, rim thickness is 18.83 mm, rim

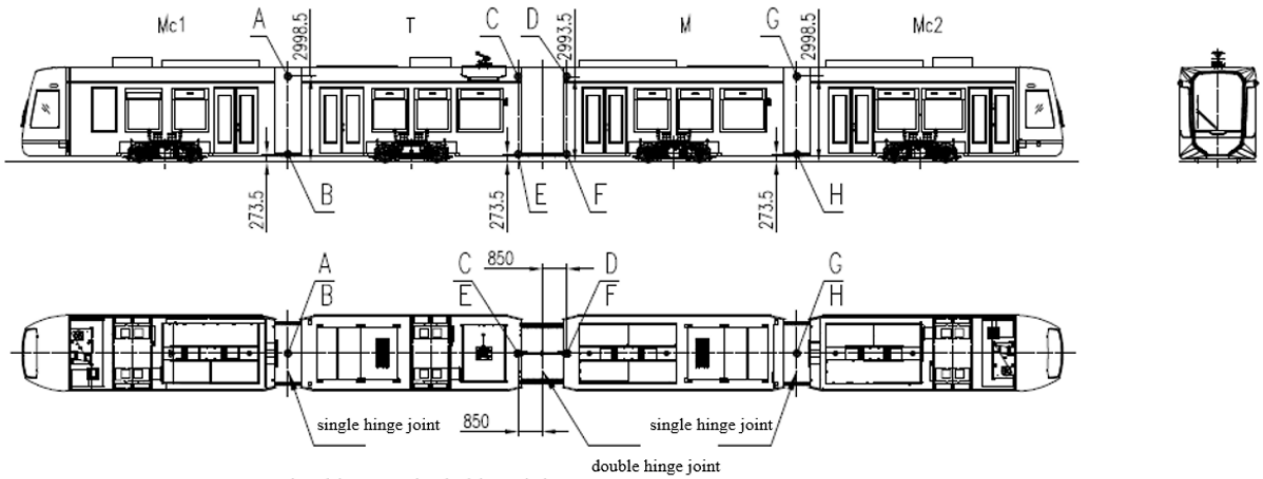

A、C: upper rotating hinge at single hinge joint

B、H: lower fixed hinge at single hinge joint

C–D: upper elastic tie rod at double hinge joint

E–F: lower fixed hinge at double hinge joint

single hinge joint: only horizontal rotational motion between vehicles is allowed

double hinge joint: allows for horizontal rotation, nodding, and rolling motions between vehicles

Fig. 6 Train formation

QR value is 4.176 mm, tread slope is 0.026, equivalent slope is 0.498, and the dimensions of the wheel profile are shown in Fig. 7 [29]. The parameter values of the train module are referred to the literature [30].

The track module is set as the continuous elastic support model, the rail is simulated by the Euler beam, and the fastener connecting the rail and track slab is simulated by the spring-damper element. The relevant parameter values for the track module are given in the literature [31, 32].

The wheel-rail contact module includes normal and tangential interactions. The normal problem is solved based on the Hertz nonlinear elastic contact theory, where the normal force p is defined as [33]:

$$p(t)=\left[\frac{1}{G}\Delta Z(t)\right]^{3/2} \tag{1}$$

where, G is the wheel-rail contact constant; $Z(t)$ is the wheel-rail contact normal elastic compression; and t is the time. For the tangential problem, the longitudinal and transverse creep forces are first calculated based on the Kalker creep theory (FASTSIM), and then corrected using the Shen's theory.

The completed numerical model of modern tram-track coupling multi-body dynamics is shown in Fig. 8, and the validity analysis of the numerical model is referred to the literature [30].

4 Formation mechanism of line corrugation

In this section, the generation cause of rail corrugation on modern tram lines is investigated. Since the structure form of the modern tram bogie (i.e., the longitudinally coupled independent wheelset bogie) is different from that of the traditional metro train, it is necessary to analyze its guiding mechanism first in order to facilitate the later explanation of the formation mechanism of rail corrugation on the corresponding line.

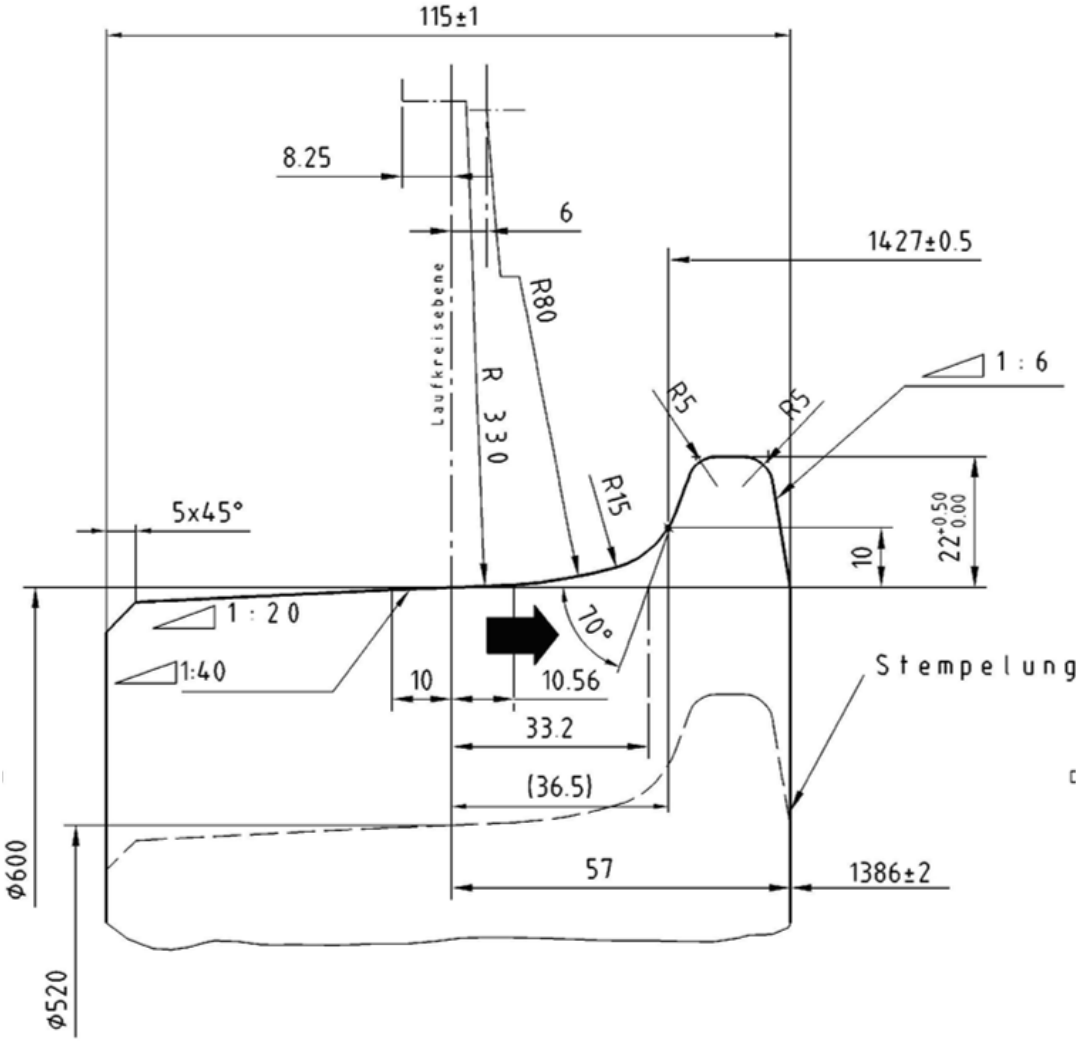

Fig. 7 Wheel profile dimensions

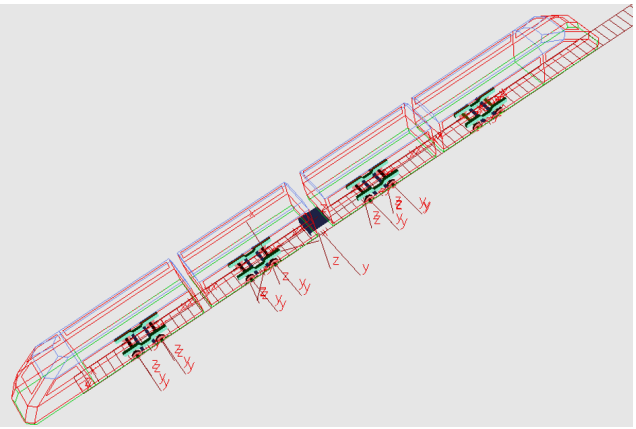

Fig. 8 Numerical model

4.1 Bogie guiding mechanism

The guiding mechanism of the longitudinally coupled independent wheelset bogie is shown in Fig. 9, where $y_i (i = 1, 2)$ is the transverse displacement of the independent wheelset in the i^{th} position and $\varphi_i (i = 1, 2)$ is the yaw angle of the independent wheelset in the i^{th} position.

When calculating creepages for the independent wheelset, the effect of the rotational velocity of the wheel on the longitudinal and transverse creepages needs to be taken into account. The longitudinal creepages and transverse creepages of the left and right wheels of the first and second wheelsets are, respectively:

$$\xi_{xiL} = -\frac{b}{v}\dot{\varphi}_i - \frac{r_{0i}}{v}\dot{\beta}_L - \frac{\lambda_i}{r_0}y_i \tag{2}$$

$$\xi_{xiR} = \frac{b}{v}\dot{\varphi}_i - \frac{r_{0i}}{v}\dot{\beta}_R + \frac{\lambda_i}{r_0}y_i \tag{3}$$

$$\xi_{yiL} = \xi_{yiR} = \frac{\dot{y}_i}{v} - \varphi_i \tag{4}$$

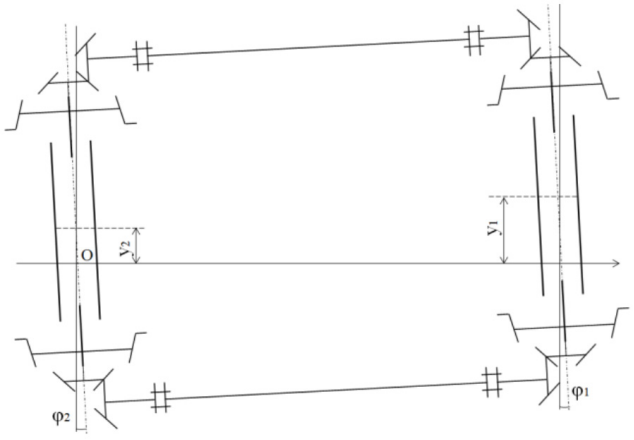

Fig. 9 Bogie guiding mechanism

where, ξ_{xiL} and ξ_{xiR} are the longitudinal creepages of the left and right wheels of the i^{th} wheelset, respectively; ξ_{yiL} and ξ_{yiR} are the transverse creepages of the left and right wheels of the i^{th} wheelset, respectively; b is the half of the transverse spacing between the rolling circles of the left and right wheels; v is the running velocity of the vehicle; r_0 is the nominal rolling circle radius of the wheel; β_L and β_R are the left and right side wheel-rail contact angles, respectively; λ is the wheel tread slope. From Eqs. (2)–(4), the longitudinal creep forces and transverse creep forces of the first and second wheelsets are, respectively:

$$F_{xiL} = -f_{11}\xi_{xiL} = -f_{11}\left(-\frac{b}{v}\dot{\varphi}_i - \frac{r_{0i}}{v}\dot{\beta}_L - \frac{\lambda_i}{r_0}y_i\right) \tag{5}$$

$$F_{xiR} = -f_{11}\xi_{xiR} = -f_{11}\left(\frac{b}{v}\dot{\varphi}_i - \frac{r_{0i}}{v}\dot{\beta}_R + \frac{\lambda_i}{r_0}y_i\right) \tag{6}$$

$$F_{yiL} = -f_{22}\xi_{yiL} = -f_{22}\left(\frac{\dot{y}_i}{v} - \varphi_i\right) \tag{7}$$

$$F_{yiR} = -f_{22}\xi_{yiR} = -f_{22}\left(\frac{\dot{y}_i}{v} - \varphi_i\right) \tag{8}$$

where, F_{xiL} and F_{xiR} are the longitudinal creep forces of the left and right wheels of the i^{th} wheelset, respectively; F_{yiL} and F_{yiR} are the transverse creep forces of the left and right wheels of the i^{th} wheelset, respectively; f_{11} and f_{22} are the longitudinal and transverse creep coefficients, respectively.

Since the spin creep is very small, under the condition of neglecting the effect of spin moment, when there are both transverse and yaw motions in the independent wheelsets, according to Kalker's linear theory, it can be seen that the longitudinal creep forces of the left and right wheels of the first and second wheelsets can be written as:

$$F_{xiL} = -f_{11}\xi_{xiL} = -f_{11}\frac{v + b\dot{\varphi}_i - \omega_L\left(r_{0i} + \lambda_i y_i\right)}{v} \tag{9}$$

$$F_{xiR} = -f_{11}\xi_{xiR} = -f_{11}\frac{v - b\dot{\varphi}_i - \omega_R\left(r_{0i} - \lambda_i y_i\right)}{v} \tag{10}$$

where ω_L and ω_R are the rolling angular velocities of the left and right wheels, respectively.

The angular velocities of the front and rear wheelsets on the same side of the longitudinally coupled independent wheelset bogie are consistently equal. When the rolling circle radii of the front and rear wheelsets deviate, the longitudinal velocities at rolling circles are no longer equal, thus generating longitudinal creep forces, and the

longitudinal creep forces of the front and rear wheelsets are equal in size and opposite in direction. According to Eq. (9) then there is:

$$F_{x1L} = F_{x2L}\,. \tag{11}$$

That is, Eq. (12) holds:

$$\frac{v + b\dot{\varphi}_1 - \omega_L\left(r_{01} + \lambda_1 y_1\right)}{v} = \frac{v + b\dot{\varphi}_2 - \omega_L\left(r_{02} + \lambda_2 y_2\right)}{v}\,. \tag{12}$$

From the above, it can be seen that there is still a possibility of the existence of the longitudinal creep force between the wheel and the rail for the longitudinally coupled independent wheelset bogie, whereas for the fully independent rotating wheels of the trailer bogie, there is no longitudinal creep force. Since the longitudinal creep force and transverse creep force are crucial for corrugation formation, the wheel-rail contact characteristics of the first wheelset of the longitudinally coupled independent wheelset bogie will be the objective of the subsequent analysis.

4.2 Corrugation formation mechanism

Rail corrugation occurs in the micro contact patch area, and is closely related to the variation characteristics of wheel-rail creep. Referring to the literatures [34, 35], when the wheel-rail resultant creepage is greater than 9.5‰, it can be assumed that the wheel-rail creep of the corresponding line section is saturated, i.e., the wheel-rail system has the possibility of corrugation occurrence, in which the resultant creepage υ is as shown in Eq. (13):

$$\upsilon = \sqrt{\xi_x^2 + \left(\xi_y + \psi a\right)^2} \tag{13}$$

where, ψ is the spin; a is the longitudinal half-axis length of the contact patch.

In view of this, this paper focuses on the resultant creepage as an evaluation index to analyze the formation mechanism of rail corrugation on modern tram line sections. Using the established multi-body dynamics numerical model and setting up the simulation conditions corresponding to the four sets of measured line sections in Section 2, the calculations are then executed separately to analyze the occurrence probability of rail corrugation in each line section from the perspective of the creepage. The multi-body dynamics numerical model can simulate, to a certain extent, vehicle operation situations and wheel-rail contact creep states under different actual line conditions, and thus the corresponding calculation results are conducive to the understanding of the formation mechanism of rail corrugation.

4.2.1 Simulation condition 1

Referring to the first set of measured line section, the track line type is set as follows: 50 m straight line + 120 m transition curve + 80 m circular curve + 120 m transition curve, the radius of the circular curve is 30 m, the curve superelevation is 0, and the passing velocity of the vehicle is 15 km/h. Through the simulation, the resultant creepages of the inside and outside wheel-rail interfaces of the first wheelset of the longitudinally coupled independent wheelset bogie can be obtained, as shown in Fig. 10.

From Fig. 10, it can be seen that in the circular curve section, the resultant creepages of the inside and outside wheel-rail interfaces are both greater than 35.0‰ and far exceed the critical value of 9.5‰, indicating that the creepages of the inside and outside wheel-rail interfaces has all reached saturation, which is easy to induce uneven wear of the inner and outer rails. Meanwhile, in the metro automatic train operation

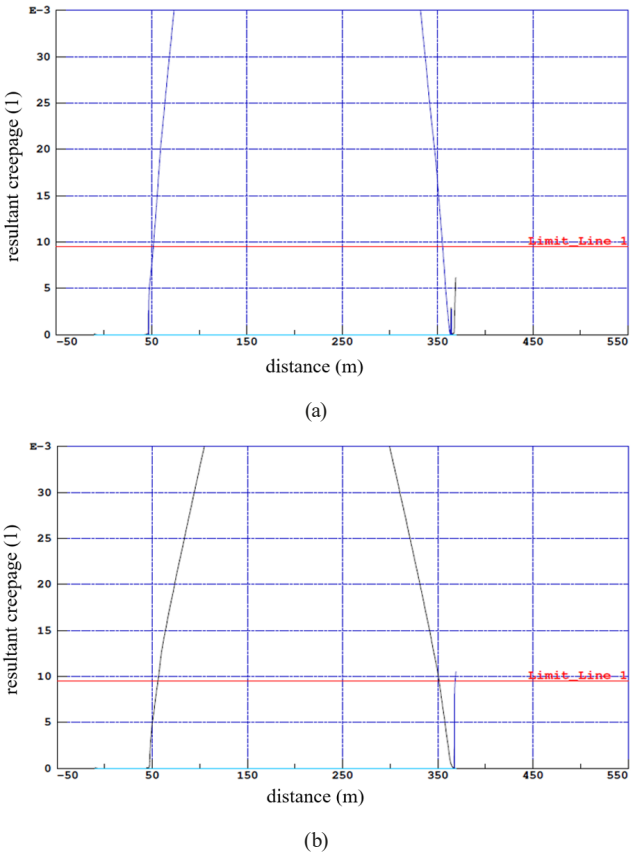

Fig. 10 Wheel-rail resultant creepages - simulation condition 1 (a) Outside wheel-rail resultant creepage (b) Inside wheel-rail resultant creepage

(ATO) mode, with the reciprocating operation of the train, the uneven wear will further evolve into the wavy wear, and eventually form the obvious corrugation phenomenon.

4.2.2 Simulation condition 2

Referring to the second set of measured line section, the track line type is set to be consistent with Section 4.2.1, the radius of the circular curve is 105 m, the curve superelevation is 0, and the passing velocity of the vehicle is 23 km/h. By performing the numerical calculation, the resultant creepages of the inside and outside wheel-rail interfaces of the first wheelset of the longitudinally coupled independent wheelset bogie obtained are shown in Fig. 11.

As can be seen in Fig. 11, in the circular curve section, the resultant creepages of the inside and outside wheel-rail interfaces exceed the critical value of 9.5‰, with the resultant creepage of the outside wheel-rail interface being greater than 35.0‰, and the resultant creepage of the inside wheel-rail interface being greater than 20.0‰. This indicates that the contact creepages at the inside and outside wheel-rail interfaces are both saturated, i.e., both the inner and outer rails have the tendency to undergo corrugation.

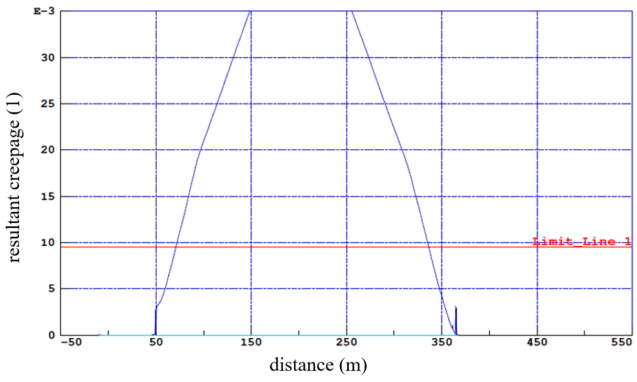

(a)

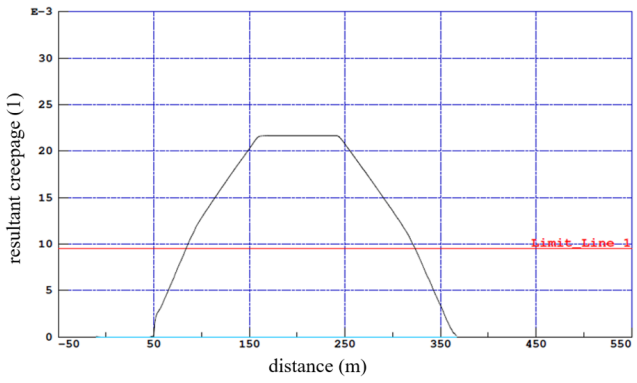

(b)

Fig. 11 Wheel-rail resultant creepages - simulation condition 2 (a) Outside wheel-rail resultant creepage (b) Inside wheel-rail resultant creepage

4.2.3 Simulation condition 3

With reference to the third set of measured line section, the track line type is set as 100 m straight line, and the passing velocity of the vehicle is 68 km/h. By calculation, the corresponding resultant creepages of the inside and outside wheel-rail interfaces can be obtained as shown in Fig. 12.

According to Fig. 12, it is easy to see that in the straight line, the inside and outside wheel-rail resultant creepages are much smaller than the critical value of 9.5‰, indicating that the inside and outside wheel-rail contact creepages are unlikely to reach saturation under ideal conditions, i.e., rail corrugation is unlikely to be formed. However, there is rail corrugation in the measured line section. In order to explain the above phenomenon, after field measurements and data analysis, it is believed that the difference in wheel diameters between the front and rear wheelsets on the same side is one of the main triggers. The difference in wheel diameters between the front and rear wheelsets on the same side will induce the longitudinal velocities of the front and rear wheelsets at rolling circles to be no longer equal, which in turn generates longitudinal creep forces

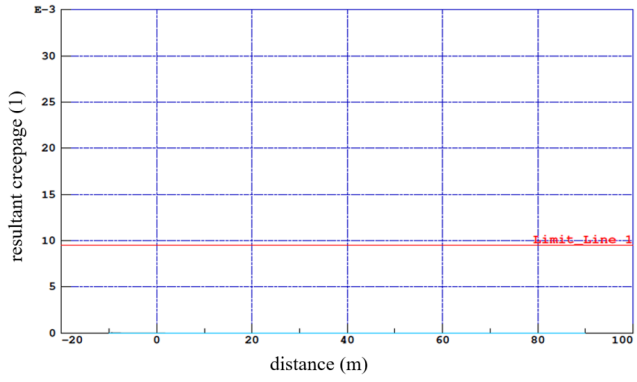

(a)

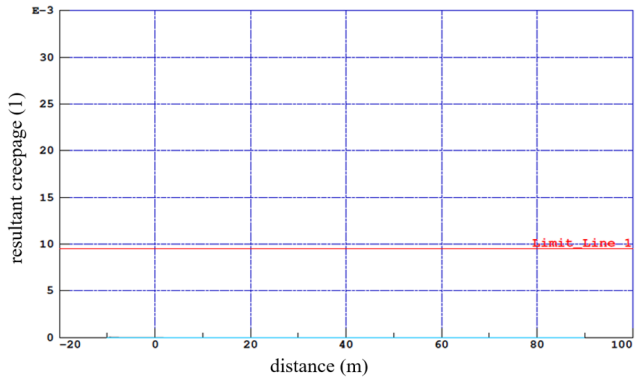

(b)

Fig. 12 Wheel-rail resultant creepages - simulation condition 3 (a) Outside wheel-rail resultant creepage (b) Inside wheel-rail resultant creepage

Table 1 Data of wheel diameters

Vehicle	Data	First Left Wheel	First Right Wheel	Second Left Wheel	Second Right Wheel
M	before re-profiling (mm)	589.24	590.04	590.19	590.73
	after re-profiling (mm)	586.28	586.24	587.08	587.12
Mc2	before re-profiling (mm)	592.03	592.34	593.07	592.64
	after re-profiling (mm)	589.90	589.79	590.59	590.53

and induces the generation of corrugation. Table 1 shows the wheel diameter data of the two cars (all of them are motors, recorded as M and Mc2, respectively), which illustrates that the difference between the front and rear wheel diameters of the M wheelsets before re-profiling is up to 1.49 mm, and the difference between the front and rear wheel diameters of the Mc2 wheelsets is up to 1.04 mm; after re-profiling, the difference between the front and rear wheel diameters of the M wheelsets reaches a maximum of 0.88 mm, and the difference between the front and rear wheel diameters of the Mc2 wheelsets reaches a maximum of 0.80 mm; therefore, it is reasonable to attribute the reason of corrugation on the straight line to the longitudinal creep forces caused by such a large difference in the front and rear wheel diameters.

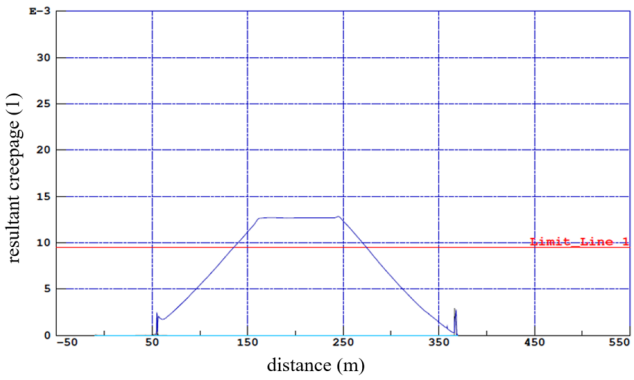

(a)

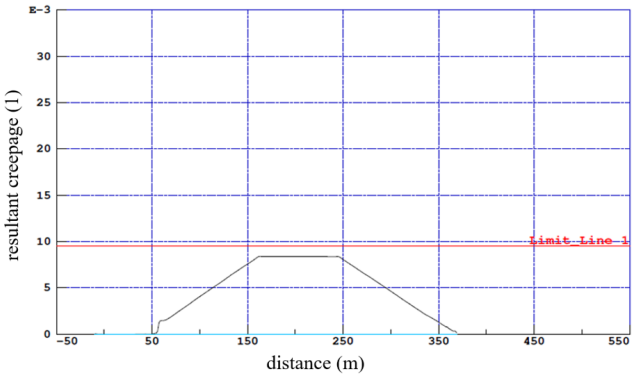

(b)

Fig. 13 Wheel-rail resultant creepages - simulation condition 4 (a) Outside wheel-rail resultant creepage (b) Inside wheel-rail resultant creepage

4.2.4 Simulation condition 4

Similarly, with reference to the fourth set of measured line section, the track line type is kept the same as in Section 4.2.1, and the radius of the circular curve is set to be 350 m, the curve superelevation is set to be 65 mm, and the passing velocity of the vehicle is set to be 61 km/h. By numerical calculation, the corresponding wheel-rail resultant creepages can be obtained as shown in Fig. 13.

According to Fig. 13, in the circular curve section, the outside wheel-rail resultant creepage (≈13.0‰) exceeds the critical value of 9.5‰, while the inside wheel-rail resultant creepage (≈8.2‰) does not exceed the critical value of 9.5‰, but it is in the vicinity of the critical value of 9.5‰, i.e., the inside wheel-rail creepage in practice also has the possibility of reaching saturation, especially in the condition of the presence of irregularities in wheel and rail surfaces. However, under ideal simulation conditions, the outside wheel-rail contact creepage is more likely to reach saturation and thus more likely to initiate outside rail corrugation.

In summary, the calculation results in Sections 4.2.1–4.2.4 are in good agreement with the measured results in Section 2, demonstrating that the phenomenon of rail corrugation on modern tram lines can be well explained from the micro perspective of wheel-rail contact. In the meantime, the formation mechanism of rail corrugation on modern tram lines can be summarized as wheel-rail contact creep saturation leading to the generation of rail corrugation, and the source of creep is related to the guiding mechanism of the longitudinally coupled independent wheelset bogie.

5 Conclusions

On the basis of the actual situation of modern tram lines, using the multi-body dynamics method, this paper establishes a modern tram-track coupling numerical model, and studies the formation mechanism of rail corrugation on measured lines from the point of view of wheel-rail contact creep by combining field investigation and numerical calculations. The main conclusions are as follows:

1. Rail corrugation on modern tram lines mainly occurs in small radius curve sections with the radius below 400 m, and the smaller the curve radius is,

the greater the occurrence probability of rail corrugation is. The corrugation wavelength ranges from 40 mm to 50 mm and the wave depth ranges from 0.05 mm to 0.1 mm. The corrugation wave depth is relatively small compared to that of the metro line, which is in line with the characteristics of light-load operation of the tram.

2. Numerical simulation shows that for the modern tram line section with the curve radius ranging from 30 m to 350 m, the contact creepages of the inside and outside wheel-rail interfaces of the first wheelset of the longitudinally coupled independent wheelset bogie all reach or are close to the saturation state, which indicates that both the inner and outer rails have the occurrence possibility of corrugation. The above results are consistent with the field measurements, illustrating that the wheel-rail contact creep saturation is the main mechanism for the formation of rail corrugation.
3. The formation of rail corrugation on the straight line of the modern tram is related to the difference in wheel diameters between the front and rear wheelsets on the same side of the longitudinally coupled independent wheelset bogie. The difference in wheel diameters between the front and rear wheelsets on the same side will lead to different longitudinal velocities of the front and rear wheelsets at rolling circles, thus generating longitudinal creep forces and inducing rail corrugation. Therefore, one potential preventive strategy for rail corrugation is to reduce the difference in wheel diameters between the front and rear wheelsets on the same side.

Since our numerical model is a multi-rigid body model and does not take into account flexibility properties of vehicle and track structures, this may limit the accuracy degree of calculation results, thus affecting the generalizability of relevant results. In view of this, future research will develop bogie (including wheelsets) and track 3D finite element models and import them into the existing numerical model to take into account the flexibility of vehicle and track structures, so as to accurately characterize wheel-rail contact creep characteristics.

Nomenclature

Symbol	Parameter and Explanation	Unit (SI)
p	normal force	N
G	wheel-rail contact constant	–
$Z(t)$	wheel-rail contact normal elastic compression	m
t	time	s
$y_i (i = 1, 2)$	transverse displacement of the independent wheelset in the i^{th} position	m
$\varphi_i (i = 1, 2)$	yaw angle of the independent wheelset in the i^{th} position	rad
ξ_{xiL}	longitudinal creepage of the left wheel of the i^{th} wheelset	–
ξ_{xiR}	longitudinal creepage of the right wheel of the i^{th} wheelset	–
ξ_{yiL}	transverse creepage of the left wheel of the i^{th} wheelset	–
ξ_{yiR}	transverse creepage of the right wheel of the i^{th} wheelset	–
b	half of the transverse spacing between rolling circles of left and right wheels	m
v	running velocity of the vehicle	m/s
r_0	nominal rolling circle radius of the wheel	m
β_L	left side wheel-rail contact angle	rad
β_R	right side wheel-rail contact angle	rad
λ	wheel tread slope	-
F_{xiL}	longitudinal creep force of the left wheel of the i^{th} wheelset	N
F_{xiR}	longitudinal creep force of the right wheel of the i^{th} wheelset	N
F_{yiL}	transverse creep force of the left wheel of the i^{th} wheelset	N
F_{yiR}	transverse creep force of the right wheel of the i^{th} wheelset	N
f_{11}	longitudinal creep coefficient	–
f_{22}	transverse creep coefficient	–
ω_L	rolling angular velocity of the left wheel	rad/s
ω_R	rolling angular velocity of the right wheel	rad/s
υ	resultant creepage	–
ψ	spin	m^{-1}
a	longitudinal half-axis length of the contact patch	m

References

[1] Li, W. "Study on root cause of metro rail corrugation and its influence on behavior of vehicle-track system", PhD Thesis, Southwest Jiaotong University, 2015.

[2] Ge, Y., Lei, S., Li, Q. "High-Frequency Resonances of Train-Track Coupled System Due to Multiple Wheels Interference", International Journal of Structural Stability and Dynamics, 23, 2340018, 2023. https://doi.org/10.1142/S0219455423400187

[3] Ren, D., Tao, G., Li, W., Wen, Z. "Short-pitch corrugation formation on resilient fastener metro tracks explained using rail-bending vibrations within the bogie wheelbase", Proceedings of the Institution of Mechanical Engineers Part F: Journal of Rail and Rapid Transit, 238(4), pp. 449–460, 2023. https://doi.org/10.1177/09544097231182748

[4] Liu, W., Zhang, H., Liu, W., Thompson, D. J. "Experimental study of the treatment measures for rail corrugation on tracks with Egg fasteners in the Beijing metro", Proceedings of the Institution of Mechanical Engineers Part F: Journal of Rail and Rapid Transit, 232(5), pp. 1360–1374, 2018. https://doi.org/10.1177/0954409717721635

[5] Wu, B. W., Chen, G. X., Lv, J. Z., Zhu, Q., Kang, X. "Generation mechanism and remedy method of rail corrugation at a sharp curved metro track with Vanguard fasteners", Journal of Low Frequency Noise Vibration and Active Control, 39(2), pp. 368–381, 2020. https://doi.org/10.1177/1461348419845992

[6] Song, Q. F., Chen, G. X., Dong, B. J., Ren, W. J., Feng, X. H. "Study on rail corrugation on curved tracks on metro ramps", Wear, 523, 204769, 2023. https://doi.org/10.1016/j.wear.2023.204769

[7] Cui, X., He, Z., Huang, B., Chen, Y., Du, Z., Qi. W. "Study on the effects of wheel-rail friction self-excited vibration and feedback vibration of corrugated irregularity on rail corrugation", Wear, 477, 203854, 2021. https://doi.org/10.1016/j.wear.2021.203854

[8] Mei, G., Chen, G. "Slip of wheels on rails: the root cause for rail undulant wear", Wear, 523, 204727, 2023. https://doi.org/10.1016/j.wear.2023.204727

[9] Grassie, S. L., Kalousek, J. "Rail Corrugation: Characteristics, Causes and Treatments", Proceedings of the Institution of Mechanical Engineers, Part F: Journal of Rail and Rapid Transit, 207(1), pp. 57–68, 1993. https://doi.org/10.1243/PIME_PROC_1993_207_227_02

[10] Grassie, S. L. "Rail Corrugation: Characteristics, Causes, and Treatments", Proceedings of the Institution of Mechanical Engineers, Part F: Journal of Rail and Rapid Transit, 223(6), pp. 581–596, 2009. https://doi.org/10.1243/09544097JRRT264

[11] Grassie, S. L. "The corrugation of railway rails: 1. introduction and mitigation measures", Proceedings of the Institution of Mechanical Engineers, Part F: Journal of Rail and Rapid Transit, 237(5), pp. 588–596, 2023. https://doi.org/10.1177/09544097221125626

[12] Grassie, S. L. "The corrugation of railway rails: 2. Monitoring and conclusions", Proceedings of the Institution of Mechanical Engineers, Part F: Journal of Rail and Rapid Transit, 237(5), pp. 597–605, 2023. https://doi.org/10.1177/09544097221122011

[13] Chen, G. X., Zhou, Z. R., Ouyang, H., Jin, X. S., Zhu, M. H., Liu, Q. Y. "A finite element study on rail corrugation based on saturated creep force-induced self-excited vibration of a wheelset-track system", Journal of Sound and Vibration, 329(22), pp. 4643–4655, 2010. https://doi.org/10.1016/j.jsv.2010.05.011

[14] Chen, G. X., Cui, X. L., Qian, W. J. "Investigation into rail corrugation in high-speed railway tracks from the viewpoint of the frictional self-excited vibration of a wheel-rail system", Journal of Modern Transportation, 24(2), pp. 124–131, 2016. https://doi.org/10.1007/s40534-016-0106-6

[15] Chen, G. X., Zhang, S., Wu, B. W., Zhao, X. N., Wen, Z. F., Ouyang, H., Zhu, M. H. "Field measurement and model prediction of rail corrugation", Proceedings of the Institution of Mechanical Engineers, Part F: Journal of Rail and Rapid Transit, 234(4), pp. 381–392, 2020. https://doi.org/10.1177/0954409719877318

[16] Matsumoto, A., Sato, Y., Ono, H., Tanimoto, M., Oka, Y., Miyauchi, E. "Formation mechanism and countermeasures of rail corrugation on curved track", Wear, 253(1–2), pp. 178–184, 2002. https://doi.org/10.1016/S0043-1648(02)00097-2

[17] Wu, T. X. "Parametric excitation of wheel/track system and its effects on rail corrugation", Wear, 265(9–10), pp. 1176–1182, 2008. https://doi.org/10.1016/j.wear.2008.01.025

[18] Chiacchiari, L., Loprencipe, G. "Measurement methods and analysis tools for rail irregularities: a case study for urban tram track", Journal of Modern Transportation, 23(2), pp. 137–147, 2015. https://doi.org/10.1007/s40534-015-0070-6

[19] Kou, L., Sysyn, M., Liu, J., Fischer, S., Nabochenko, O., He, W. "Prediction system of rolling contact fatigue on crossing nose based on support vector regression", Measurement, 210, 112579, 2023. https://doi.org/10.1016/j.measurement.2023.112579

[20] Herráiz, J. I. R., Morales-Ivorra, S., Zamorano Martin, C., Soler Basauri, V. "Analysis of Vibrations Generated by the Presence of Corrugation in a Modeled Tram Track", Mathematical Problems in Engineering, 2015, 290164, 2015. https://doi.org/10.1155/2015/290164

[21] Bethel Lulu, G., Chen, R., Wang, P., Xu, J., Chen, J., Fang, J. "Random vibration analysis of tram-track interaction on a curve due to the polygonal wheel and track irregularity", Vehicle System Dynamics, 60(4), pp. 1125–1147, 2022. https://doi.org/10.1080/00423114.2020.1847299

[22] Mandula, J., Salaiová, B., Koval'aková, M. "Prediction of noise from trams", Applied Acoustics, 63(4), pp. 373–389, 2002. https://doi.org/10.1016/S0003-682X(01)00047-0

[23] Csortos, G., Augusztinovicz, F., Bocz, P. "Optimal operation of a rail lubrication device with respect to noise reduction and wheel/rail friction coefficient", Acta Technica Jaurinensis, 14(2), pp. 138–154, 2021. https://doi.org/10.14513/actatechjaur.00592

[24] Csortos, G., Augusztinovicz, F., Kazinczy, L. "Examination of Rail Dampers with Respect to Noise and Vibration Mitigation", Periodica Polytechnica Civil Engineering, 64(3), pp. 658–667, 2020. https://doi.org/10.3311/PPci.13382

[25] Jóvér, V., Fischer, S. "Statistical analysis of track geometry parameters on tramway line No. 1 in Budapest", The Baltic Journal of Road and Bridge Engineering, 17(2), pp. 75–106, 2022. https://doi.org/10.7250/bjrbe.2022-17.561

[26] Jóvér, V., Major, Z., Németh, A., Kurhan, D., Sysyn, M., Fischer, S. "Investigation of the Geometrical Deterioration of Paved Superstructure Tramway Tracks in Budapest (Hungary)", Infrastructures, 8(8), 126, 2023. https://doi.org/10.3390/infrastructures8080126

[27] Wang, Y. "Theoretical investigation into the measurability of rail unevenness and corrugation using the dynamic response of axle box and bogie", Proceedings of the Institution of Mechanical Engineers, Part F: Journal of Rail and Rapid Transit, 235(3), pp. 275–285, 2021. https://doi.org/10.1177/0954409720923213

[28] Santa, J. F., Toro, A., Lewis, R. "Correlations between rail wear rates and operating conditions in a commercial railroad", Tribology International, 95, pp. 5–12, 2016. https://doi.org/10.1016/j.triboint.2015.11.003

[29] Zhu, L., Xu, H. "The study on the influence of wheel diameter difference on the stability of independent wheelset bogie", Modern Transportation Technology, 17(4), pp. 78–81, 2020.

[30] Huang, Y. H., Fu, M. H. "100% Low-floor vehicles of CSR Zhuzhou Electric Locomotive Co., Ltd.-calculation report of dynamic performances", Southwest Jiaotong University, Chengdu, China, 2014.

[31] Zhang, Z., Yang, X.-W., Ma, K.-K., Zhao, Z.-J., Lu, W.-X. "Study on relationship between fastener system mode and rail corrugation of modern tram line", Engineering Mechanics, 38(12), pp. 249–256, 2021. https://doi.org/10.6052/j.issn.1000-4750.2020.12.0906

[32] Wang, Z., Lei, Z. "Formation Mechanism of Metro Rail Corrugation Based on Wheel–Rail Stick–Slip Behaviors", Applied Sciences-Basel, 11(17), 8128, 2021. https://doi.org/10.3390/app11178128

[33] Cai, X., Tan, X., Guo, L. Zhong, Y. "Spatial Distribution Characteristics of Rail Vibration Acceleration under Train Load", Journal of Southwest Jiaotong University, 53(3), pp. 459–466, 2018. (in Chinese) https://doi.org/10.3969/j.issn.0258-2724.2018.03.005

[34] Persson, I. "GENSYS. 2001 reference manual", DEsolver AB, Stockholm, Sweden, 2020. [online] Available at: https://www.gensys.se/

[35] Kalker, J. J. "Three-Dimensional Elastic Bodies in Rolling Contact", Springer Dordrecht, 1990. ISBN 978-0-7923-0712-9 https://doi.org/10.1007/978-94-015-7889-9